Finite Element Modeling of Cyclic Behavior of Shear Wall Structure Retrofitted using GFRP

by Z.J. Li, T. Balendra, K.H. Tan, and K.H. Kong

Synopsis: In this paper, a non-linear 3-D finite element analysis (FEA) model using ABAQUS (Hibbit, Karlsson and Sorensen, Inc. 2003) was developed to predict the cyclic behavior of shear wall structures. In this FEA model, SPRING element is used to simulate the constraint deformation due to fiber reinforced polymer (FRP) wrapping, and improved concrete stress-strain curve is considered to account for the improvement of strength and ductility of concrete under FRP confinement. A damaged plasticity-based concrete model is used to capture the behavior of concrete under cyclic loading. Method to identify shear failure due to FRP debonding and FRP rupture in FEA is also proposed. The model is validated using the results from the experimental study. It is shown that the proposed model can predict the shear failure and cyclic hysteresis behavior of GFRP-wrapped shear wall reasonably well.

Keywords: cyclic behavior; fiber-reinforced polymer; finite element analysis; glass fibers; retrofitting; seismic; shear strength; shear wall

Z.J. Li is a research scholar and phd candidate in the Department of Civil Engineering at National University of Singapore. He has received his Master degree in South China University of Technology. His current research interests inculde seismic behavior of structures and seismic retrofitting using FRP.

T. Balendra is a professor in civil engineering at the National University of Singapore. He received his phd degree from Northwestern University in USA. His current research interests include performance and retrofitting of seismic resistant structures.

ACI member K.H. Tan is an associate professor in civil engineering at National University of Singapore where he received his MEng degree. He received his phd degree from the University of Tokyo. His current research interests include FRP systems, structural composites and structural strengthening.

K.H. Kong is a research fellow in civil engineering department at National University of Singapore, where he received his PHD degree. His current research interests include: earthquake engineering, structural analysis, structural concrete design and high strength light weight concrete.

INTRODUCTION

During recent earthquakes (e.g. 1994 Northridge earthquake in the USA, 1995 Kobe earthquake in Japan, and 2003 Bam earthquake in Iran), many old buildings designed without seismic provisions suffered severe damages. As a result, seismic retrofitting of old buildings has attracted more attention. The traditional seismic retrofit methods, such as adding new shear wall or infilled wall, steel jacketing and concrete caging, have disadvantages to some extent, for example, adding mass to the footing and labor and equipment intensive. In recent years, seismic retrofit using FRP has become a promising alternative to the traditional seismic retrofit methods due to the excellent characteristic of FRP such as high strength to weight ratio, immunity to corrosion, easy and fast installation.

Although considerable research work has been carried out on FRP for seismic application, most of the literature only reported experimental investigations and some analytical analyses, but seldom discussed FEA (finite element analysis) modeling (Laursen et al. 1995; Lombard et al. 2000; Ma and Xiao 1997; Matsuzaki et al. 2000; Restrepo et al. 1998; Seisble et al. 1997; Haroun et al. 2001; Ye et al. 2001). This may be due to the difficulties of FEA modeling, for example, in capturing the cyclic behavior of concrete, modeling concrete-FRP interface, identifying the failure of FRP, and simulating the behavior of FRP.

Recently, for monotonic loading, FEA models of FRP retrofitted structures have been proposed. Buyle-Bodin et al. (2002) proposed a 2D FEA model using the French Code Castem2000 (developed by CEA, French nuclear research center) to analyze the flexural behavior of externally bonded CFRP (carbon FRP) RC structures under pushover loading. In this model, the internal steel bars as well as the CFRP plates were modeled using two-node bar linear elements. The model could simulate CFRP bonding and the results compared well with the test results. Kong et al. (2003) proposed a 3D finite-element model using program ABAQUS to simulate shear walls wrapped with GFRP (glass FRP). In their model, FRP was modeled using SHELL element and the results of FEA matched well with the test results. Eusebio et al (2002) used software DIANA (2000) to perform 2D FEA modeling of FRP retrofitted masonry panles. They used SPRING element to simulate the constraint on deformation provided by FRP strips. However, they did not consider the improvement of concrete strength due to FRP confinement.

In this paper, a 3D FEA modeling using program ABAQUS for cyclic behavior of FRP retrofitted shear walls is being proposed. In this FEA modeling, SPRING element is used to simulate the constraint on deformation provided by FRP strips. The improvement in strength of concrete core due to FRP confinement is also considered. A concrete model based on damaged plasticity is used to capture the cyclic behavior of concrete. And a failure criterion of FRP retrofitted structures is proposed. The modeling is validated using the experimental results (Z.J. Li et al. 2004).

RESEARCH SIGNIFICANCE

The nonlinear 3D FEA model using ABAQUS proposed herein provides researchers and designers with a computational tool for design of GFRP retrofitted shear wall structures. Through FEA modeling, the failure mode, the failure location, the extent of strength and ductility improvement due to the chosen number FRP layers can be obtained. Therefore, with the proposed FEA modeling, it is possible for designers to do trial and error analysis until an effective and reasonable retrofit scheme is achieved.

FEA MODELING

Overview of the physical model

A 1/5 scale model of the lower 2.6 story shear wall of a 25-story building in Singapore is considered. This model, when wrapped with GFRP, was tested previously by Li et al. (2004) under cyclic loading. The wall is an I-shaped wall with two flange walls and one center wall. The thickness of the wall is 45mm throughout. The length of the center wall is 955mm, the length of the flange wall is 657mm, and the height of the wall is 1314mm. (as shown in Figure 1). The lateral cyclic load (the loading history is shown in Figure 2) was transferred from the actuator to the wall through the upper loading transfer beams. The rate of cyclic loading changed twice: 0.006mm/s in the first 3 cycles (maximum top displacement is 3mm,6mm and 9mm,respectively); 0.01mm/s in the fourth cycle(maximum top displacement is 12mm), and 0.05mm/s in the finial cycles (maximum top displacement is 15mm twice and 30mm twice).

The longitudinal reinforcing bars in the center wall and the mid portion of the flange wall are 8mm diameter smooth high yield steel bars ($f_y = 525$ MPa). The longitudinal reinforcing bars in the edge portion of the flange wall and the base block are 10mm diameter deformed high yield steel bars ($f_y = 480$ MPa). The horizontal bars in the wall are 6mm smooth mild steel bars ($f_y = 350$ MPa). The cube compressive strength at the day of test was f_{cu}=27.58MPa. A layer of unidirectional Glass FRP (Mbrace EG900 glass fiber reinforced polymer) was used to wrap the specimen. GFRP bolts were used at the flange wall-web wall joints to anchor GFRP sheets and then the anchor parts were covered by GFPR sheets. Thickness of the GFRP sheets is 0.353mm, and Young's module is 69.65GPa. The ultimate tensile strength of GFRP is 1667.7MPa and the ultimate tensile strain is 0.02.

Overview of the FEA model

A total of 220 elements of C3D8R type (8 node solid brick elements with one Gaussian integration point) were used to model the tested wall. The 3-D view of the meshing of the RC wall is shown in Figure 3. Steel reinforced bars in the concrete wall were modeled as one-directional strain elements (rods) and were simulated by rebar option. In ABAQUS, when rebar option is used, the steel reinforcing bars will be superposed on a mesh of standard element types, like C3D8R type element. The concrete behavior of walls will be considered independent of the reinforcing bars. The effects associated with the rebar-concrete interface, like bond slip and dowel action, are normally modeled approximately by introducing some "tension stiffening" into the concrete modeling. The reinforcing bars were superimposed onto the wall. SPRING element was used to model the constraint on deformation provided by wrapping FRP. Totally 525 SPRING elements were used.

The boundary condition of the base of the wall was simulated as fixed end. In order to prevent out-of-plane displacement, roller supports were placed at each node of the surface of brick elements 37, 38, 107 and 108. A vertical pressure load was applied on flange and web of the top elements to simulate the vertical load. Lateral concentrated point loads were applied on each of the top node on the flange walls to simulate the lateral cyclic displacement shown in Figure 2.

Laws of materials

The steel reinforcing bars were considered as elastic perfectly plastic materials in both tension and compression. The assumed uniaxial stress-strain curve of the steel bars is shown in Figure 4. The main parameters of steel materials like yield strength, Young's modulus and ultimate strength were obtained from the experimental study. The stiffness of the SPRING element was equal to that of the GFRP material (69.65GPa).

A new concrete model (Concrete Damaged Plasticity model) in ABAQUS version 6.3 was used to simulate the behavior of concrete of the walls. This model is a continuum plasticity-based damage model for concrete. It assumes that the two main failure mechanisms are tensile cracking and compressive crushing of the concrete material, and that the uniaxial tensile and compressive response of concrete is characterized by damaged plasticity. Under uniaxial tension, the stress-strain response follows a linear elastic relationship until the failure stress σ_{t0}, which represents the onset of micro-cracking in the concrete material. Beyond this failure stress, the formation of micro-cracks is represented macroscopically with a softening stress-strain response. On the other hand, under uniaxial compression the response is linear until the value of initial yield, σ_{c0}. In the plastic regime the response is typically characterized by stress hardening followed by strain softening beyond the ultimate stress, σ_{cu}. When the concrete specimen is unloaded from any point on the strain softening branch of the stress-strain curves, the unloading response is weakened and the elastic stiffness of the material is damaged. The degradation of the elastic stiffness is characterized by two damage variables, d_t and d_c ($0 \le d_{t,} d_c \le 1$). Under cyclic loading conditions the degradation mechanisms are quite complex, involving the opening and closing of previously formed micro-cracks and their interaction. The stiffness recovery effect, namely some recovery of the elastic stiffness as the load changes sign in cyclic test, is considered. The weight factors, w_t and w_c, control the recovery of the tensile and compressive stiffness upon load reversal, respectively. w_c, which results in the recovery of the compressive stiffness, is more important because when the load changes from tension to compression, tensile cracks will close. The whole model described above is shown in Figure 5.

The stiffness recovery factors were chosen as the default values: $w_t = 0$ and $w_c = 1$. For the tension stiffening effect, CONRETE TENSION STIFFENING TYPE=STRAIN option (more suitable for concrete with reinforcement) was used and the reduction of concrete tensile strength to zero is assumed to occur at 10 times the strain at failure.

The compression stress-strain curve of concrete was calculated by the formula proposed by Teng (2001), considering the improvement of concrete strength and strain due to GFRP confinement. The improved concrete stress-strain curve proposed by Teng(2001) is shown in Figure 6.

The improved stress-strain relationship (the parameters are denoted in Figure 6) is:

$$\begin{cases} \sigma_c = E_c \varepsilon_c - \dfrac{(E_c - E_2)^2}{4 f_{co}'} \varepsilon_c^{\,2} & (0 \le \varepsilon_c \le \varepsilon_t) \\ \sigma_c = f_{co} + E_2 \varepsilon_c & (\varepsilon_t \le \varepsilon_c \le \varepsilon_{cc}) \end{cases} \tag{1}$$

where

$$\varepsilon_t = \frac{2 f_{co}'}{(E_c - E_2)}$$

$$E_2 = \frac{f_{cc}' - f_{co}'}{\varepsilon_{cc}}$$

$$\frac{\varepsilon_{cc}}{\varepsilon_{co}} = 2 + k_2 \frac{f_l}{f_{co}'} \quad \text{(For E-glass FRP, } k_2 = 26.7\text{)}$$

$$f_l = \frac{2 f_{frp} t_{frp}}{\sqrt{h^2 + b^2}}$$

$$\frac{f_{cc}'}{f_{co}'} = 1 + k_1 k_s \frac{f_l'}{f_{co}'} \quad k_1 = 2 \quad \text{(Confinement effectiveness coefficient)}$$

$$f_l' = k_s f_l ,$$

$$k_s = \frac{b}{h} \frac{A_e}{A_c}$$

$$\frac{A_e}{A_c} = \frac{1 - [(b/h)(h - 2R_c)^2 + (h/b)(b - 2R_c) h^2]/(3A_g) - \rho_{sc}}{1 - \rho_{sc}}$$

ρ_{sc} = Reinforcement bar ratio

b =Width of the rectangular concrete core

h =Height of the rectangular concrete core

According to Tan (2002), the whole concrete can be divided into several regions of concrete core separated by the internal transverse links, because the internal links provide additional anchor points and help in restraining the concrete from bulging out. Since the shear wall under investigation is an I shape wall, FRP bolts were used to anchor the flange wall-web wall joints (Li et al. 2004). Thus, FRP bolts can be considered as the internal transverse links, and the I shape wall can be divided into 4 rectangular regions as shown in Figure 7. Equation (1) was used to calculate the improved strength stress-strain curve for concrete of each region, since different region had different width and height. The calculated compression stress-strain curves of these four-region concrete are shown in Figure 8.

The parameters of concrete used in the FEA modeling like Young's module, compressive strength, were obtained from the experimental study.

Parameters to identify failure in FEA study

The equations for shear given in ACI 318 code (2002) were used to identify the shear failure of the RC shear wall. In ACI 318 code, for members subjected to additional axial compression force, the shear capacity of concrete is:

$$v_c = (1 + \frac{N_u}{14A_g})(\frac{\sqrt{f_c'}}{6}) \text{ MPa} \quad (2)$$

where, N_u is the axial compression force and A_g the area of the cross section.

The shear capacity provided by the horizontal steel reinforcement is:

$$v_s = \frac{A_v f_y d}{s_2 A_s} \text{ MPa} \quad (3)$$

where, A_v is area of horizontal shear reinforcement within a vertical distance s_2 and horizontal distance d, A_s the area of shear surface.

The equation of shear capacity of FRP wrap is derived by Triantafillou (2000) is:

$$v_f = 0.8 E_f \varepsilon_f \rho_f \text{ MPa} \quad (4)$$

where,

E_f = Young's modulus of fiber

ε_f =effective FRP strain at failure which is calculated as 0.0025 (FRP rupture) and 0.002 (FRP debonding) (Kong et al., 2003).

ρ_f =FRP shear reinforcement ratio, which is $\frac{2t_f}{b_w}$ for continuously bonded shear reinforcement with thickness t_f.

t_f =thickness of the fiber.

D =length of flange wall.
b_w =thickness of flange wall.

Thus, the shear capacity of reinforced concrete without FRP retrofitted can be calculated using:

$$v = v_c + v_s = (1 + \frac{N_u}{14A_g})(\frac{\sqrt{f_c'}}{6}) + \frac{A_v f_y d}{s_2 A_s} \tag{5}$$

And the shear capacity of RC shear wall retrofitted using FRP can be calculated using

$$v = v_c + v_s + v_f = (1 + \frac{N_u}{14A_g})(\frac{\sqrt{f_c'}}{6}) + \frac{A_v f_y d}{s_2 A_s} + 0.8E_f \varepsilon_f \rho_f \tag{6}$$

Based on formulas (2) to (6), the shear capacity of the RC flange wall was calculated as 1.74MPa, and the shear capacity before FRP debonding and FRP rupture were 3.49MPa and 3.93MPa, respectively.

COMPARISON BETWEEN TEST AND FEA

Analysis of shear failure

In the experimental study, yielding of the steel reinforcement occurred first at the bottom of the outmost 10mm deformed bar when top displacement was 10.11mm and corresponding force was 192.52kN (4th cycle). The first FRP debonding appeared at the left flange wall corner and at the right flange wall corner, when the displacement was 15mm (5^{th} cycle). With increase in displacement, more debonding occurred, and the concrete corner began to spall and crush. Finally, after the first 30mm peak displacement was passed and the opposite direction displacement of 23.5mm was reached (7^{th} cycle), the right flange wall concrete corner crushed abruptly and the nearby FRP debonded dramatically (as shown in Figure 9). The failure mode of the specimen was shear failure with FRP debonding followed by FRP rupture.

In FEA modeling, the 1st flexural crack (shear stress> shear capacity of reinforced concrete=1.74MPa) occurred at 53.6kN when the top lateral displacement was 0.75mm (1st cycle). As shown in Figure 10, at this stage, the shear stress of some of the critical regions in the flange wall started to exceed the shear capacity of reinforced concrete, and the additional shear force will be sustained by FRP. As shown in Figure 11, the first debonding of FRP (shear stress> shear capacity due to FRP debonding 3.49MPa) occurred at the corner region of the shorter flange wall in the third cycle (9mm displacement cycle). However, the debonding region was very small in the third and fourth cycles (9mm and 12mm displacement cycles), this is why in the experiment no FRP debonding was observed until the fifth cycle (15mm displacement cycle). In the fifth and sixth cycles (twice 15mm displacement cycle), the region of debonding developed dramatically as shown in Figure 12. As can be seen from Figure 12, the regions of debonding are mainly at the corner of the flange wall and the nearby regions. This matches well with the regions of debonding in the test. The final shear failure due to FRP rupture in the 7th cycle (30mm displacement cycle) (shear stress> shear capacity due to FRP rupture 3.93MPa) is shown in Figure 13. The FRP rupture regions concentrated at the corners of flange wall and nearby regions as what had been observed in the test.

Thus, FEA proposed previously can predict the shear failure of the shear wall tested quite well.

Analysis on global scale

In the tested shear wall specimen, micro-cracks exist due to shrinkage effects of concrete. Such micro-cracks will reduce the stiffness, the initial stiffness and the stiffness in the process of loading, of the tested specimen. For the scaled models, such influence will be amplified due to size effect (Elnashai et al 1990; Kong et al 2003). In ABAQUS, such micro-cracks cannot be modeled, and thus when comparing the FEA results with the test results, the influence of the micro-cracks should be accounted. For this purpose, the displacement of FEA needs to be amplified by a factor of 4, which was obtained by dividing the ultimate stiffness of test results by that of the FEA analysis.

The cycle by cycle comparison of the top lateral force-displacement curves between the test and FEA is shown in Figure 14. As can be seen from Figure 14, FEA modeling could predict the shape of the hysteresis force-displacement curves reasonably well. It is noted that the proposed FEA modeling underestimated the lateral force to some extent. However, considering the variation of materials in the test, such error is acceptable.

CONCLUSION

A 3D non-linear finite element model with SPRING elements to account for the improvement of strength and ductility of concrete under FRP confinement is proposed. This model predicts the failure mode and the overall hysterestic behavior of GFRP retrofitted shear wall structures reasonably well.

REFERENCES

ACI 318, 2002, Building code requirements for structural concrete and commentary.

Buyle-Bodin F., David E. and Ragneau E., 2002, "Finite Element Modelling of Flexural Behaviour of Externally Bonded CFRP Reinforced Concrete Structures," *Engineering Structures* V. 24 , pp. 1423-1429.

DIANA, 2000, *User Manual-DIANA Version 7*, DIANA Analysis, P.O. Box 113, 2600 AC Delft, The Netherlands.

Elnashai A.S, Pilakoutas K., Ambraseys N.N.,1990, "Experimental Behavior of reinforced concrete walls under earthquake loading," Earthquake Engineering and Structural Dynamics. V. 19. pp. 389-407.

Eusebio M., Palumbo. P., Lozza F. and Manfredi G., 2002, "Numerical Modelling of Masonry Panels Strengthened Using FRPs," *Finite Elements in Civil Engineering Applications*, Swets& Zeitlinger, Lisse, Hendriks & Rots (Ed.), pp. 295-303.

Haroun M. A., Mosallam A. S., Feng M. Q. and Elsanadedy H. M., 2001, "Experimental Investiation of Seismic Repair and Retrofit of Bridge Columns by Composite Jackets," *Proceedings of the International Conference on FRP Composites in Civil Engineering*, Dec 12-15 2001, Hong Kong, China, pp. 839-848.

Hibbit, Karlsson and Sorensen, Inc., 2003, *ABAQUS/Standard user's manual (Version 6.3)*, Pawtucket, RI.

Kong K. H.; Tan K. H.; and Balendra, T., 2003, "Retrofitting of shear walls designed to BS 8110 for seismic loads using FRP," *Proceedings of the Sixth International Symposium on FRP Reinforcement for Concrete Strictires(FRPRCS-6)*, Tan. K. H (ed.), July 8-10, 2003, Singapore, Vol. 2, pp. 1127-1136.

Laursen P. T.; Seibel F.; Hegemier G. A.; and Innamorato D., 1995, "Seismic Retrofit and Repair of Masonry Walls with Carbon Overlays," *Non-metallic (FRP) reinforcement for concrete structures* , E&FN Spon, Taerwe L. (ed.), pp. 617-623.

Li, Z.J.m;   K.H. Kong; T. Balendra; and K.H. Tan, 2004, "Behaviour of FRP retrofitted shear walls designed according to BS8110," *Developments in Mechanics of Structures & Materials*, Australia, Andrew J. Deeks and Hong Hao (eds), pp. 133-137

Lombard J. C.; Lau D. T.; Humar J. L.; Cheung M. S.; and Foo S., 2000, "Seismic Repair and strengthening of Reinforced Concrete Shear Walls for Flexure and Shear using Carbon Fibre Sheets," *Advanced Composite Materials in Bridges and Structures, Montreal*, The Canadian Society for Civil Engineering, Humar J. and Razaqpur A. G (eds), pp. 645-652.

Ma, R., and Xiao, Y., 1997, "Seismic Retrofit and Repair of Circular Bridge Columns with Advanced Composite Materials," *Earthquake Spectra,* V. 15, No. 4, pp. 747-764.

Matsuzaki Y.; Nakano K.; Fujii S.; and Fukuyama H., 2000, "Seismic Retrofit using Continuous Fiber sheets," *Proceedings 12th World Conference on Earthquake Engineering*, New Zealand, pp. 2524-2531.

Restrepo J. I.; Wang Y. C.; Irwin R. W.; and Devino B., 1998, "Fibreglass/epoxy Composites for the Seismic Upgrading of Reinforced Concrete Beams with Shear and Bar Curtailment Deficiencies," *Proceedings 8th European Conference on Composite Materials*, Naples, Italy, pp. 59-66.

Seisble F.; Priestley M. J. N.; Hegemier G. A.; and Innamorato, D., 1997, "Seismic Retrofit of RC Columns with continuous Carbon Fiber Jackets," *Journal of Composites for Construction (ASCE)*, V. 1, No. 2, pp. 52-62.

Tan K. H., 2002, "Strength Enhancement of Rectangular Reinforced Concrete Columns using Fiber-Reinforced Polymer," *Journal of Composites for Construction*, V. 6, No. 3, Aug. 1, pp. 175-183.

Teng J. G.; Chen J. F.; Smith S. T.; and Lam, L., 2001, *FRP-strengthened RC structures*. New York : Wiley.

Triantafillou and Antonopoulus., 2000, "Design approach for concrete members strengthened in shear with FRP," *ASCE Journal of Composites for Construction*.

Ye, L. P.; Zhao, S. H.; Zhang, K.; and Feng, P., 2001, "Experimental Study on Seismic Strengthening of RC Columns with Wrapped CFRP Sheets," *Proceedings of the International Conference on FRP Composites in Civil Engineering*, Dec. 12-15, 2001, Hong Kong, China, pp. 885-892.

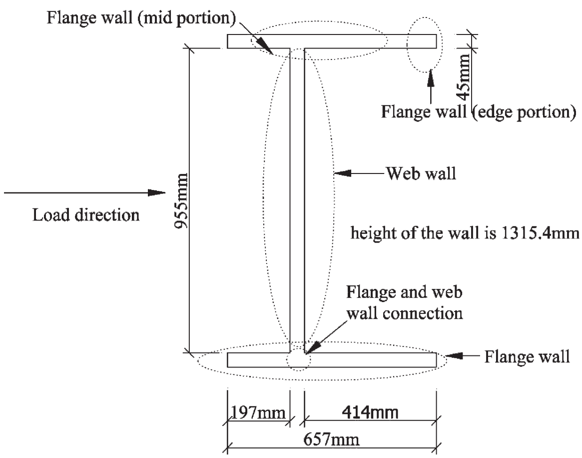

Figure 1— Plan view and geometry of the tested model

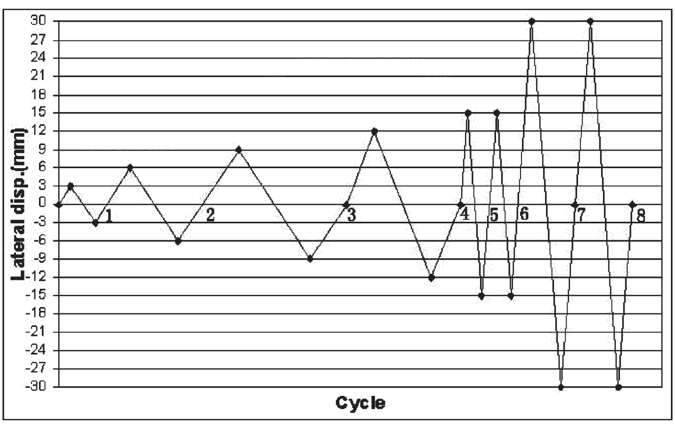

Figure 2— Cyclic loading history

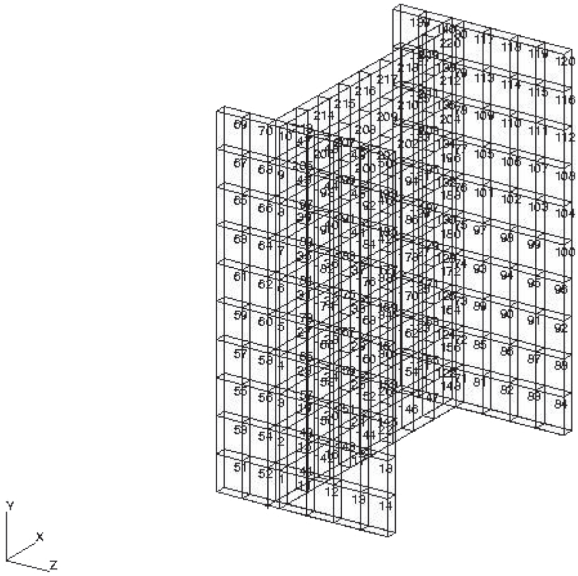

Figure 3— 3-D view of the modeling of the reinforced concrete wall

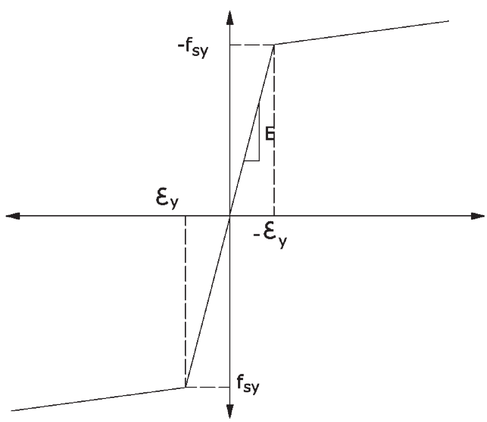

Figure 4— Stress-strain curve for steel used in ABAQUS

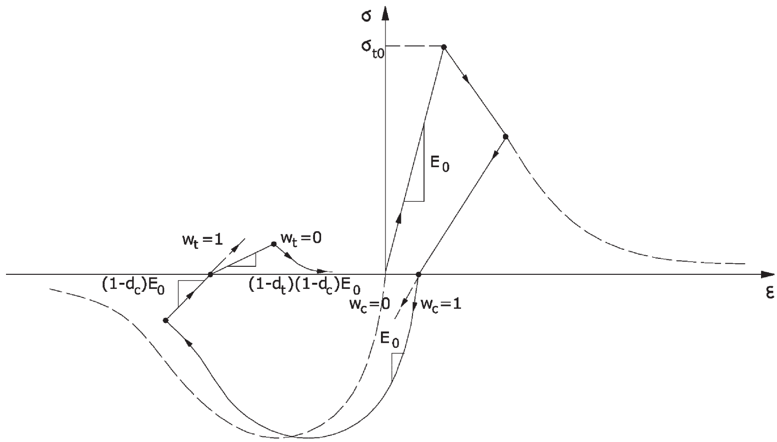

Figure 5— Stress-strain curve of concrete damaged plasticity model used in ABAQUS

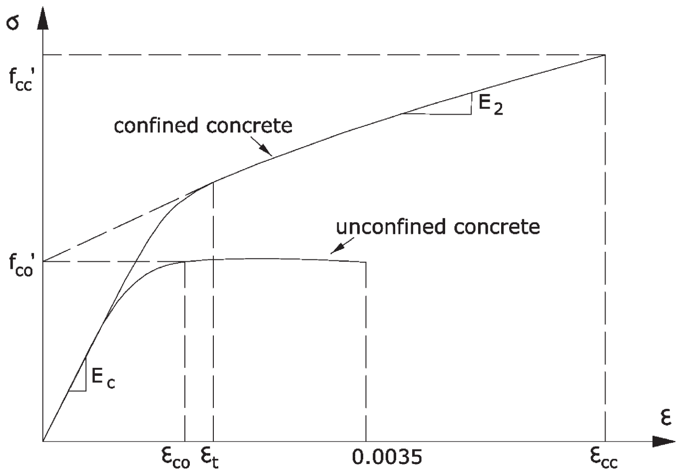

Figure 6— Stress-strain curve of improved strength of confined concrete (Teng 2001)

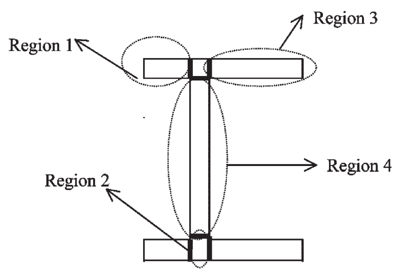

Figure 7— Wall divided into regions

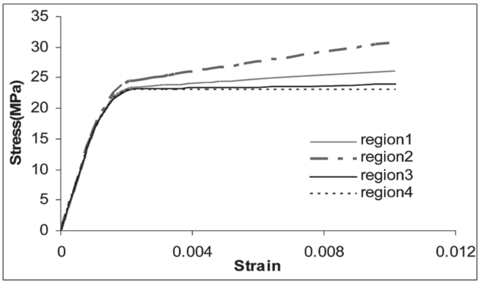

Figure 8— Stress-strain curves for confined concrete of different regions

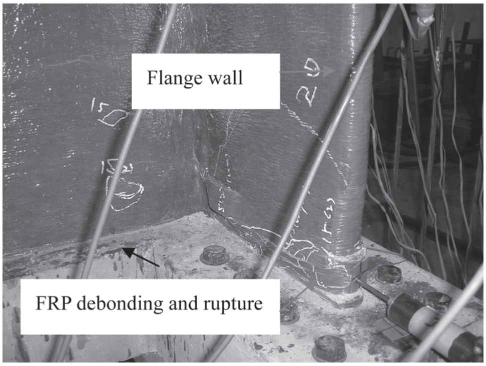

Figure 9— Failure mode of the specimen: FRP debonding followed by FRP rupture (Z.J. Li et al. 2004)

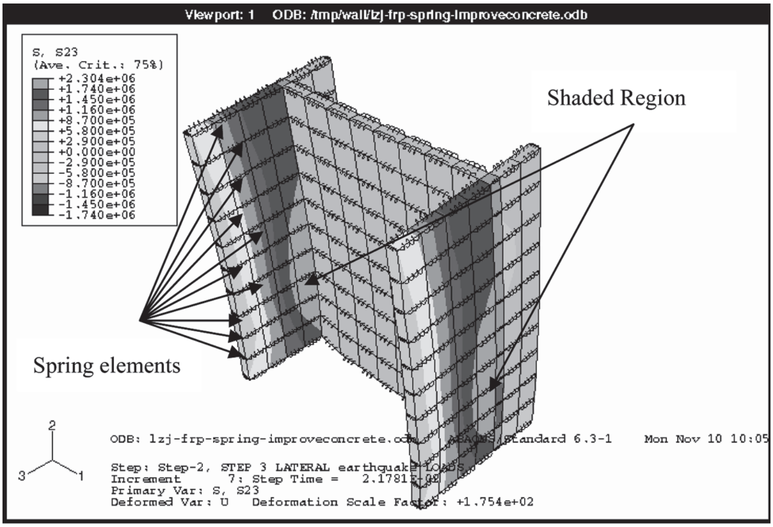

Figure 10— Initial shear failure in reinforced concrete flange wall at 53.6kN. Shade region has shear stress > 1.74 MPa (shear capacity of reinforced concrete)

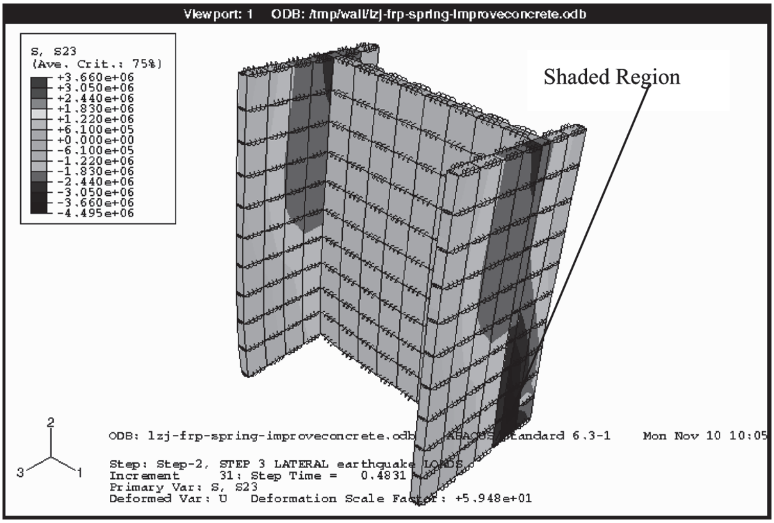

Figure 11— Initial shear failure due to FRP debonding at the 9mm displacement cycle. Shade region has shear stress > 3.49 MPa (FRP debonding shear capacity)

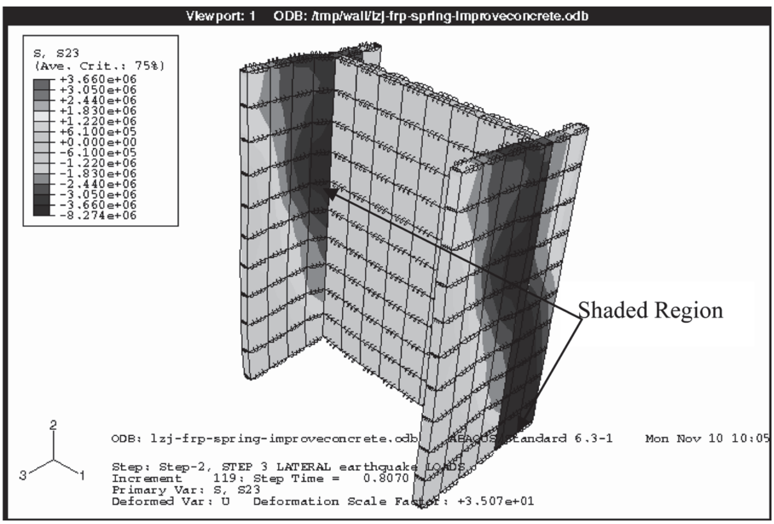

Figure 12—Shear failure due to FRP debonding at the 15mm displacement cycle. Shade region has shear stress > 3.49 MPa(FRP debonding shear capacity)

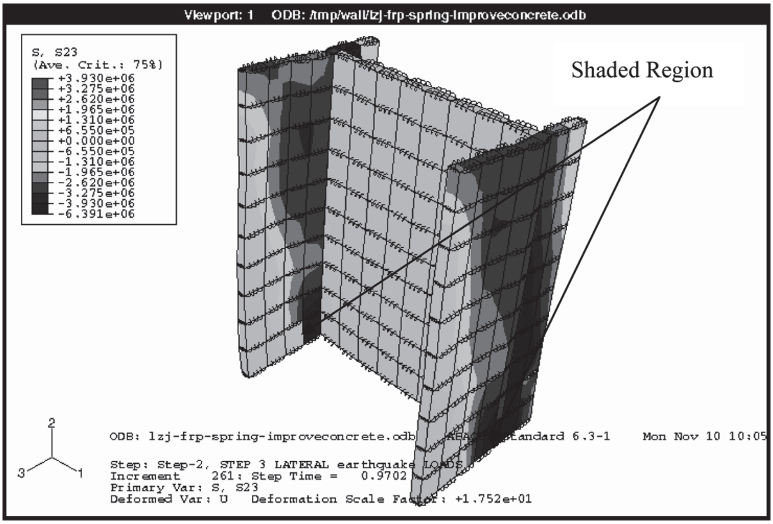

Figure 13—Shear failure due to FRP rupture (At the end of 30mm displacement cycle, lateral force was 151.78kN) Shade region has shear stress › 3.93 MPa (FRP rupture shear capacity)

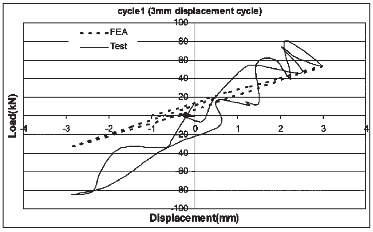

(a) Cycle 1

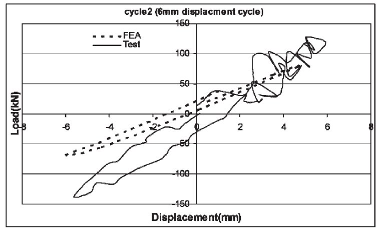

(b) Cycle 2

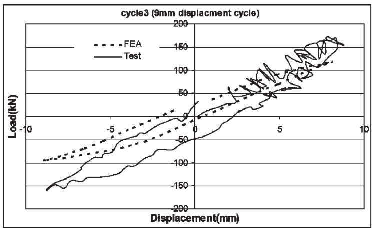

(c) Cycle 3

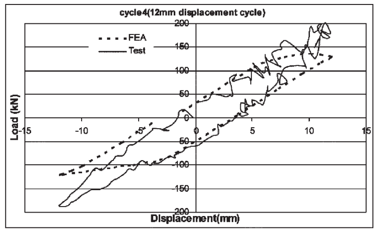

(d) Cycle 4

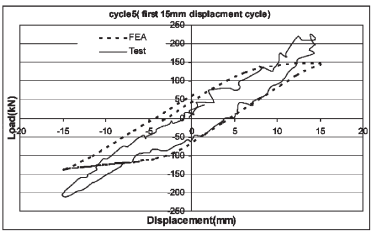

(e) Cycle 5

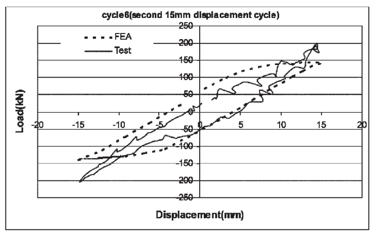

(f) Cycle 6

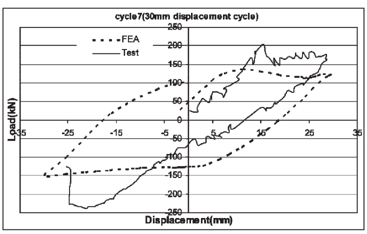

(g) Cycle 7

Figure 14—Cycle-by-cycle comparison between experiment and finite element analysis (displacement of FEA amplified by a factor of 4 to consider size effect)